Copy 6
RM E51H29

NACA RM E51H29

NACA

RESEARCH MEMORANDUM

PRESSURE RECOVERY, DRAG, AND SUBCRITICAL STABILITY CHARACTERISTICS OF CONICAL SUPERSONIC DIFFUSERS WITH BOUNDARY-LAYER REMOVAL

By Leonard J. Obery, Gerald W. Englert
and Theodore J. Nussdorfer

Lewis Flight Propulsion Laboratory
Cleveland, Ohio

NATIONAL ADVISORY COMMITTEE
FOR AERONAUTICS

WASHINGTON

February 27, 1952

NATIONAL ADVISORY COMMITTEE FOR AERONAUTICS

RESEARCH MEMORANDUM

PRESSURE RECOVERY, DRAG, AND SUBCRITICAL STABILITY CHARACTERISTICS OF CONICAL SUPERSONIC DIFFUSERS WITH BOUNDARY-LAYER REMOVAL

By Leonard J. Obery, Gerald W. Englert, and

Theodore J. Nussdorfer

SUMMARY

The external and internal aerodynamic characteristics of two conical inlets having different cowl-lip positions and employing boundary-layer bleed on the cone surface were investigated in the Lewis 8- by 6-foot supersonic wind tunnel. Data from a cold-flow investigation at zero angle of attack are presented for a range of mass-flow ratios; free-stream Mach numbers of 1.7, 1.9, and 2.0; and a Reynolds number of approximately 5×10^6 based on inlet diameter.

The results indicate that an inlet whose source of instability is cone-surface boundary-layer separation may be stabilized by bleeding off that boundary layer. The beneficial effects of the boundary-layer bleed were not accompanied by a severe penalty in drag in the increased portion of the stable range.

INTRODUCTION

Previous studies of supersonic inlets have shown that a severe pulsing problem exists in the subcritical range of diffuser operation. Some results of an inlet investigation presented in references 1 and 2 indicate instability originating from two sources: (1) a vortex sheet entering the inlet, and (2) separation of the cone-surface boundary layer. This separation is caused by the magnitude of the pressure gradient in the region of the normal shock. Significant improvement in the subcritical stable range of operation, where the source of instability was the separated boundary layer, is reported for inlets incorporating boundary-layer removal in references 2, 3, and 4.

This investigation was conducted in the NACA Lewis 8- by 6-foot supersonic wind tunnel on a 16-inch-diameter ram-jet engine designed for project Rigel to verify the effectiveness of boundary-layer removal

on a large scale model and to obtain an indication of the drag penalty imposed on the engine by a boundary-layer bleed system. Two inlets, both with boundary-layer removal on the conical portion of the center body but with different cowl-lip positions, were evaluated. These inlets were designed according to the small scale results of reference 4. The pressure-recovery and drag characteristics for both configurations are compared with the results reported in reference 1 for a similar inlet having no cone-boundary-layer removal.

The data presented were obtained with cold flow at free-stream Mach numbers of 1.7, 1.9, and 2.0 at zero angle of attack. The Reynolds number based on the inlet diameter was approximately 5×10^6.

APPARATUS AND PROCEDURE

A diagramatic sketch of a 16-inch ram-jet engine is shown in figure 1. Downstream of the inlet attachment station, the component parts of the ram-jet engine and the test apparatus were the same as those reported in reference 1. Upstream of this station, the two inlets of this investigation were the same except for 1/2-inch difference in cowl length as shown in figure 2.

The inlets may be identified by the cone half-angle and the cowl-lip position angle, such as 20-26.2 for the forward lip inlet and 20-26.0 for rearward lip inlet. Nonaerodynamic considerations required the long spike projection shown in figure 2 and thereby forced the inlets to capture only about one-half the full free-stream tube defined by the inlet diameters. Thus the inlets are essentially of the low mass-flow ratio type within the range of this investigation. Profile coordinates for the two inlets are given in table I and body dimensions downstream of the inlet attachment station are presented in table II. The boundary-layer bleed height for both inlets was 0.090 inch, which corresponds to a flow area of approximately 3 percent of the maximum free-stream tube area. The mass flow through the boundary-layer bleed duct could be varied by a remotely controlled butterfly valve. Because of space limitations, the bleed air flow could not be evaluated.

Preliminary investigation of the inlets indicated that the stable operating range was less than anticipated. The addition of half-conical windshields on the cowl outer surface over the exit of the boundary-layer bleed ducts increased the pressure ratio across the bleed system and extended the stable range to the expected values; however, no change in total drag of the configuration was detectable. All data presented were therefore obtained with the windshields.

A 0.375-inch-diameter pitot-static tube extended $4\frac{1}{2}$ inches upstream of the cone apex. The effects of this tube on the boundary-layer characteristics of the cone were neglected in the analysis of the data.

As an indication of the maximum mass air flow obtainable with each inlet, a table of ratios of the maximum free-stream tube area to the combustion-chamber area for the three free-stream Mach numbers is included in figure 2. The rearward lip inlet spilled somewhat more air supersonically than the forward lip inlet.

The method of data reduction are described in reference 1.

SYMBOLS

The following symbols are used in this report:

A_{max}	maximum cross-sectional area of engine (1.483 sq ft)
$A_{w,s}$	wetted area of spike (1.096 sq ft)
$A_{w,e}$	wetted area of engine (5.74 sq ft)
C_D	drag coefficient, $\frac{D}{q_0 A_{max}}$
D	drag (lb)
M	Mach number
m	mass flow (slugs/sec)
m/m_{max}	ratio of mass flow to maximum mass flow measured at a given stream condition
P	total pressure (lb/sq ft absolute)
p	static pressure (lb/sq ft absolute)
q	dynamic pressure, $\frac{\gamma}{2} pM^2$ (lb/sq ft)
R	radius (in.)
v	velocity
y	radial distance (in.)
β	ratio of maximum mass flow at given condition to mass flow in free stream having an area equal to cone inlet area ($\rho_0 v_0 A_c$)

[redacted]

γ	ratio of specific heats
δ	boundary-layer height
ρ	density

Subscripts:

a	additive drag
b	boundary-layer bleed drag
f	friction drag
l	local
p	pressure drag
0	free stream
1	diffuser inlet
3	combustion-chamber inlet (annular area minus longeron area) (1.034 sq ft)
4	combustion-chamber station 4 (1.394 sq ft)
5	combustion-chamber outlet
6	nozzle outlet

RESULTS AND DISCUSSION

The data obtained in this investigation are presented in terms of internal as well as external flow considerations. The internal flow will be discussed primarily on the basis of diffuser pressure-recovery characteristics and the external flow will be presented in terms of total and component drags.

Pressure-Recovery Characteristics

Over-all diffuser pressure recovery. - The variation of total-pressure recovery P_3/P_0 for both inlets is shown in figure 3 as a function of the mass-flow ratio m/m_{max}, where m_{max} is the maximum measured mass flow at the given Mach number. Also presented for comparison purposes is the stable range of a similar inlet without boundary-layer bleed, discussed in reference 1.

[redacted]

Removing the cone-surface boundary layer considerably increased the stable subcritical range of the diffuser, especially at the higher Mach numbers. In terms of mass-flow ratio, the stable subcritical range for both bleed-type inlets varied little with free-stream Mach number over the range investigated. The rear lip configuration consistently gave a greater stable subcritical range.

An explanation for the effectiveness of a boundary-layer-removal system is contained in the schlieren photographs presented in figure 4. The terminal shock for the minimum stable subcritical points for both inlets at $M_0 = 1.7$ (points A and B of fig. 3) is located the same distance upstream of the bleed gap for both inlets. The rearward lip inlet, having a greater distance between the bleed gap and the cowl lip, had a greater subcritical stable range. The action of the bleed duct was to remove a major portion of the separated boundary layer and to cause reattachment of the remaining part to the cone surface downstream of the bleed inlet. A further reduction in the mass flow created a larger separated region and allowed separated flow to enter the diffuser. Thus, as the mass flow was reduced, greater amounts of low-energy air entered the inlet causing a decrease in the total-pressure ratio across the inlet and eventually instability in the flow (see reference 5).

The effect on diffuser performance of cone boundary-layer bleed is presented in figure 5 as a function of a mass-flow ratio parameter $(m/m_{max})\beta$, where β is the ratio of the maximum mass flow to the mass flow in a free-stream tube having an area equal to the cowl-inlet area. The maximum engine mass flow remained independent of bleed air flow indicating that removing the boundary layer changed the effective cone angle and thereby compensated for the loss in mass flow through the boundary-layer bleed. The maximum pressure recovery was decreased by closing the bleed valve and the stable subcritical range was limited to the same order of magnitude as the comparative inlet of reference 1.

Throughout this investigation of low mass-flow ratio inlets the source of instability originated from the intersection of the inlet terminal shock with the boundary layer on the cone surface. Reference 2 states that this intersection forms a lambda shock pattern from the fork of which a vortex sheet is generated. It also states that the entrance of this vortex sheet into the inlet at a radius slightly less than the cowl-lip radius is the mechanism by which instability arises. No vortex sheet was observed, however, on any of the schlieren photographs taken of the inlets of this investigation. It appears that low-energy air entering the inlet near the center-body radius was sufficient to cause pulsing.

Subsonic pressure recovery. - The subsonic pressure recovery defined as the pressure recovery from the cowl lip (station 1) to the combustion-chamber inlet (station 3) is shown in figure 6 as a function of the mass-flow ratio m/m_{max}. In the stable operating range the subsonic recoveries were approximately the same for both inlets at any given flow

condition. As would be expected, the subsonic pressure recovery varied inversely with diffuser-inlet Mach number. At the minimum stable subcritical point for a Mach number of 2.0, where the inlet Mach number to the subsonic diffuser was also a minimum, no measurable subsonic loss was observed.

Inlet-pressure profiles. - The total-pressure profiles at station 1 are presented in figure 7 for the case of the boundary-layer bleed control fully open. Three flow conditions are represented: critical, minimum stable subcritical, and pulsing where applicable. For all stable flow conditions, the profiles were reasonably constant across the channel, indicating that the separated boundary-layer air was being effectively removed.

Pulsing caused a decrease in local pressure recovery but did not appreciably change the shapes of the profiles. This indicates that pulsing was accompanied by separation of the flow from the cone surface, which spread over the entire inlet area rather than being limited to only a restricted area near the inner portion of the annulus. The schlieren photograph of the forward lip inlet at a free-stream Mach number of 2.0 (fig. 8) shows a portion of the pulsing cycle where this extreme separation exists. The frequency of pulsations were approximately 9 cycles per second and the static-pressure fluctuation at station 3 in percentage of the free-stream total pressure varied from 37 percent at a free-stream Mach number of 1.7 to 54 percent at a Mach number of 2.0.

Boundary layer on cone. - As part of the investigation of the forward lip inlet, boundary-layer total-pressure rakes were mounted approximately 1 inch upstream of the bleed. Measured boundary-layer profiles for several flow conditions (fig. 9) are compared with profiles predicted by the compressible viscous-radial-flow theory of reference 6. The measured Mach numbers outside the boundary layer were in excellent agreement with inviscid-conical-flow theory and the Mach number distribution in the boundary layer was approximated by radial-flow theory for all free-stream Mach numbers. The boundary-layer profiles predicted from the theory of reference 6 were in close agreement with those predicted by the incompressible turbulent conical-boundary-layer theory of reference 7.

Calculation of the friction drag on the cone surface, based on the change in momentum of the boundary layer, indicates that the friction-drag coefficient was approximately 0.0035, based on combustion-chamber area, or 0.0047, based on the wetted area of the spike, at critical flow conditions. The theoretical friction drag of reference 6 based on wetted area ranged from 0.0032 at $M_0 = 1.7$ to 0.0036 at $M_0 = 2.0$ as compared with a constant value of 0.0035 calculated by use of the theory of reference 7.

Closing the boundary-layer bleed at critical flow conditions (fig. 9(b)) caused a general thickening of the boundary layer on the cone surface. Inspection of related schlieren photographs shows this

[redacted]

boundary layer to pass over the bleed system and enter the inlet. This, in part, accounts for the decreased pressure recovery in the stable subcritical flow range (fig. 5).

Drag Characteristics

The total-drag characteristics were obtained from force measurements with the wind-tunnel balance system by the method described in reference 1. The tare forces and boattail drags were removed so that values for drag coefficient correspond to an engine having a cylindrical constant-area combustion chamber. All drag coefficients are based upon the maximum frontal area of the ram-jet engine. No change in drag could be measured because of the addition of the windshields over the boundary-layer bleed-duct outlets.

2292

Total-drag coefficient (force measurements). - The variation of total-drag coefficient for both bleed inlets is presented in figure 10 as a function of mass-flow ratio parameter $(m/m_{max})\beta$ at free-stream Mach numbers of 1.7, 1.9, and 2.0. The drag coefficients at critical conditions were approximately the same for both inlets and showed only slight variations with free-stream Mach number.

Pressure-drag coefficient. - The cowl pressure-drag coefficient, which is an integration of the pressure coefficients along the external cowl surface, varied linearly with the mass-flow ratio m/m_{max} in the stable subcritical range for both inlets (fig. 11). Free-stream Mach number had a negligible effect upon the value of pressure-drag coefficient in the range from 1.7 to 2.0. The greater drag coefficient for the forward lip inlet was due to the greater projected area of the cowl compared with the rearward lip inlet.

Additive-drag coefficient. - The theoretical (reference 8) and experimental variation of additive-drag coefficient with mass-flow ratio is presented in figure 12. The experimental values of additive drag, calculated from the change in momentum of the engine air flow from free stream to the inlet station, are reasonably well predicted by the theory throughout the stable subcritical range.

Friction-drag coefficient. - The friction-drag coefficient $C_{D,f}$ was obtained from reference 1 for a similar configuration without boundary-layer removal. Within the limits of experimental accuracy the friction-drag coefficient was found to remain independent of free-stream Mach number and mass-flow ratio at the value of 0.063, based on engine frontal area. Basing this friction-drag coefficient on wetted area resulted in a value of 0.0016, which shows good agreement with compressible flat-plate theory of reference 9 (0.00158 at $M_0 = 1.7$).

Summation of drag components. - The summation of the individual drag components is presented in figure 13 together with the measurements of the total-drag coefficient from the tunnel-balance system. The

difference between the summated drag components and the drag obtained from force measurements is partly the contribution to the total drag imposed by the boundary-layer bleed system and partly experimental error in the determination of component drags. The drag due to the boundary-layer bleed system has been estimated for the forward lip inlet at critical mass flow by assuming that all the boundary layer on the cone as measured by the cone rakes flowed through the bleed gap. The drag of the boundary-layer bleed was then determined from the condition that all the momentum in the drag direction entering the bleed inlet was lost. These points are shown summated with the other component drags on figure 13 for the forward lip inlet and, except at the highest Mach number, show excellent agreement with the measured force readings. No cone-boundary-layer measurements were made on the rearward lip inlet and hence no bleed-drag data are presented. The convergence of the summated and the measured drag curves indicates that in the extended stable subcritical range (the region where the bleed was operating efficiently) the drag of the boundary-layer bleed system becomes small.

CONCLUSIONS

An investigation was conducted with two low mass-flow ratio inlets having different cowl-lip positions and employing boundary-layer removal on the cone surface on a 16-inch ram-jet engine. From operation over a range of mass-flow ratios at zero angle of attack and at Mach numbers of 1.7, 1.9, and 2.0, the following conclusions may be drawn:

1. A cone-boundary-layer bleed is effective in increasing the stable range of an inlet when the instability arises from separated boundary layer on the cone surface.

2. Irrespective of the distance of the bleed gap from the cowl lip, instability results for a given Mach number when the normal shock is the same maximum distance from the bleed gap for both inlets.

3. A boundary-layer bleed system may be employed without adding a severe penalty in drag in the increased portion of the stable range.

Lewis Flight Propulsion Laboratory
National Advisory Committee for Aeronautics
Cleveland, Ohio

REFERENCES

1. Nussdorfer, Theodore J., Obery, Leonard J., and Englert, Gerald W.: Pressure Recovery, Drag, and Subcritical Stability Characteristics of Three Conical Supersonic Diffusers at Stream Mach Numbers from 1.7 to 2.0. NACA RM E51H27 , 1952.

2. Ferri, Antonio, and Nucci, Louis M.: The Origin of Aerodynamic Instability of Supersonic Inlets at Subcritical Conditions. NACA RM L50K30, 1951.

3. Beil, W. J.: Results of Series III, Free-Jet Tests of the 7.81-Inch Diameter Model of the XSSM-N-6 Project Rigel Ramjet at OAL during the Period 28 November to 16 December, 1949. Rep. 5002, Marquardt Aircraft Co., March 21, 1950. (Grumman Aircraft Engr. Corp. Purchase Order B-43477 under BuAer Contract NOa(s) 9403).

4. Fisher, R. E.: Controlling the Subcritical Stability of Conical Shock Inlets. Presented at the Symposium on the Aerodynamics of Ramjet Supersonic Inlets at Wright-Patterson Air Force Base (Dayton), Oct. 3rd and 4th, 1950. Marquard Aircraft Co.

5. Sterbentz, William H., and Evvard, John C.: Criterions for Prediction and Control of Ram-Jet Flow Pulsations. NACA RM E51C27, 1951.

6. Tucker, Maurice: Approximate Turbulent Boundary-Layer Development in Plane Compressible Flow along Thermally Insulated Surfaces with Application to Supersonic-Tunnel Contour Correction. NACA TN 2045, 1950.

7. Gazley, C., Jr.: Theoretical Evaluation of the Turbulent Skin Friction and Heat Transfer on a Cone in Supersonic Flight. Rep. R49A0524, Gen. Elec. Co., Nov. 1949. (Project Hermes (TU1-2000A) U.S. Army Ordnance.)

8. Sibulkin, Merwin: Theoretical and Experimental Investigation of Additive Drag. NACA RM E51B13, 1951.

9. de Kármán, Th.: The Problem of Resistance in Compressible Fluids. Quinto Convegno "Volta", Reale Accademia d'Italia (Roma), Sett. 30-Ott. 6, 1935, pp. 3-57.

[redacted]

TABLE I - INLET COORDINATES

Distance from cone apex (in.)	Inner body diameter (in.)	Forward lip inlet cowl diameter (in.)		Rearward lip inlet cowl diameter (in.)	
		Outer surface	Inner surface	Outer surface	Inner surface
0	0				
	Conical				
	to				
12.065	9.002				
12.565		12.42	12.420		
13.065		12.81	12.66	12.75	12.75
13.48	9.980	13.13	12.90	13.05	12.94
14.35		13.82	13.36	13.69	13.36
15.35	11.040	14.20	13.70	14.20	13.70
16.85	11.400	14.44	13.94	14.44	13.94
18.35	11.520	Straight	Straight	Straight	Straight
21.13	11.700	taper to	taper to	taper to	taper to
	Constant				
26.35	to	15.28	14.78	15.28	14.78
31.49	11.700	15.64	15.14	15.64	15.14

NACA

TABLE II - COORDINATES FOR AFTERBODY OF

16-INCH RAM-JET ENGINE

Distance from attachment station (in.)	Inner body diameter (in.)	Outer body outside diameter (in.)
0	11.70	15.64
24.75	11.70	16.50
40.00	11.13	
68.39	10.08	
74.28	9.78	Constant
81.14	8.96	
86.82	7.75	
	Conical to	to
100.89	3.43	
101.61		16.500 Straight taper to
106.61		16.250 Constant to
159.98		16.250

NACA

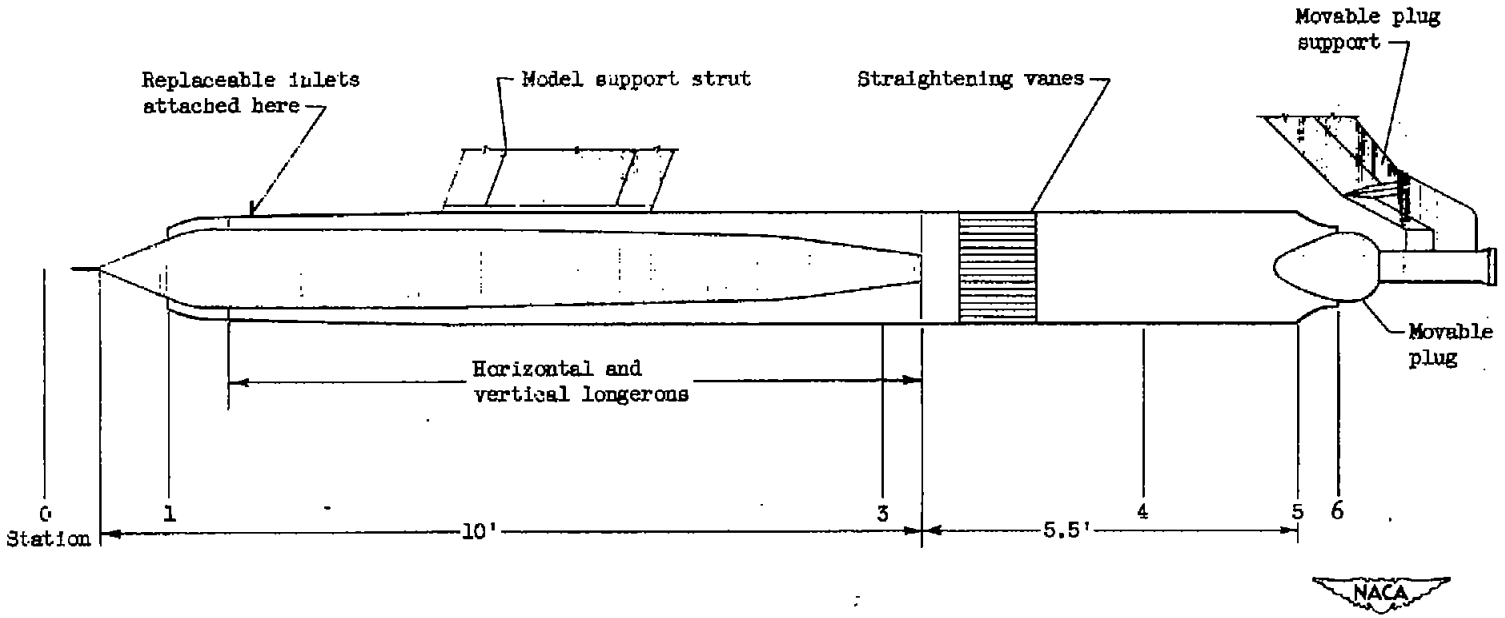

Figure 1. - Diagrammatic sketch of 16-inch ram-jet engine.

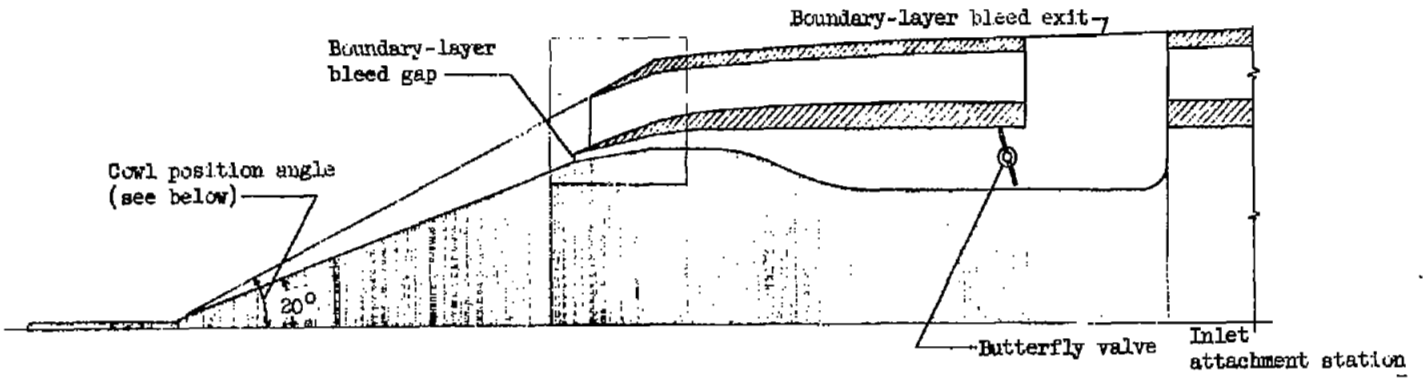

(a) Horizontal section view.

Inlet	M_0		
	1.7	1.9	2.0
	$A_{0,max}/A_e$		
Forward lip	0.302	0.324	0.332
Rearward lip	.283	.297	.306

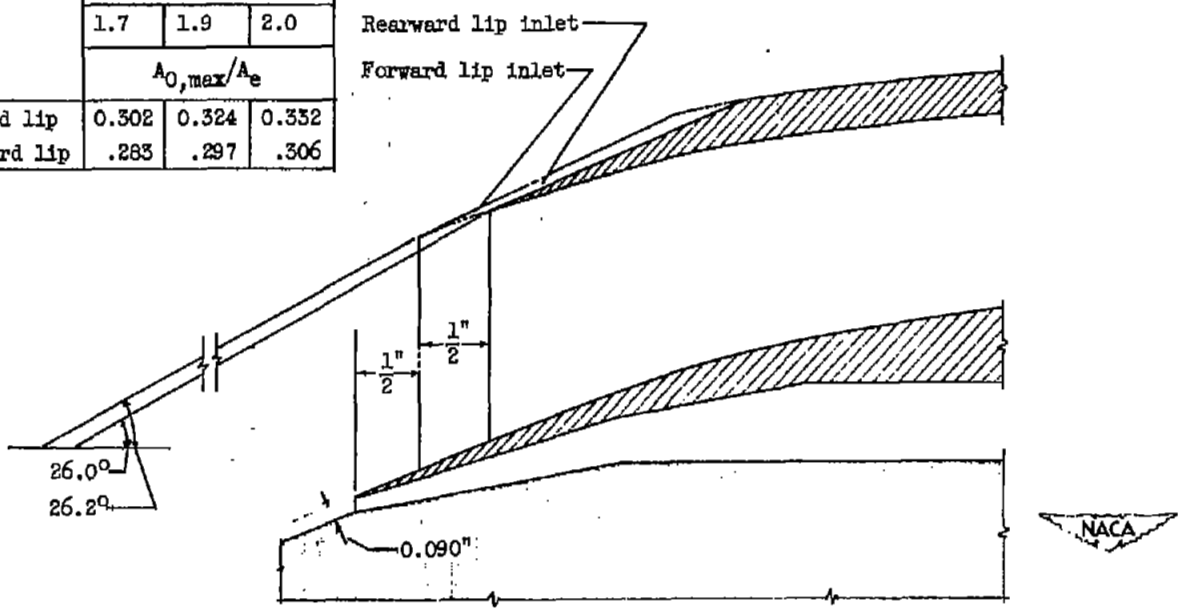

(b) Enlarged view of inlet region.

Figure 2. - Diagrammatic sketch showing geometry of inlets. $A_{0,max}/A_e$ is equal to maximum free-stream tube area divided by maximum combustion-chamber area.

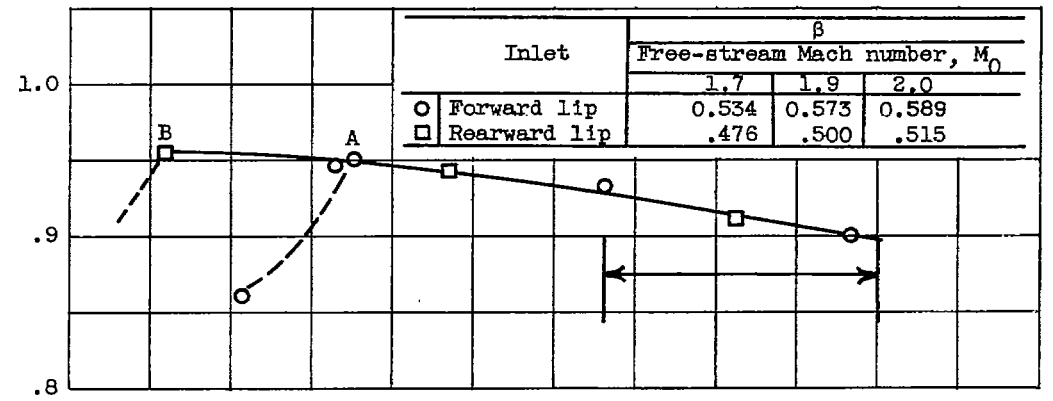

(a) Free-stream Mach number, 1.7.

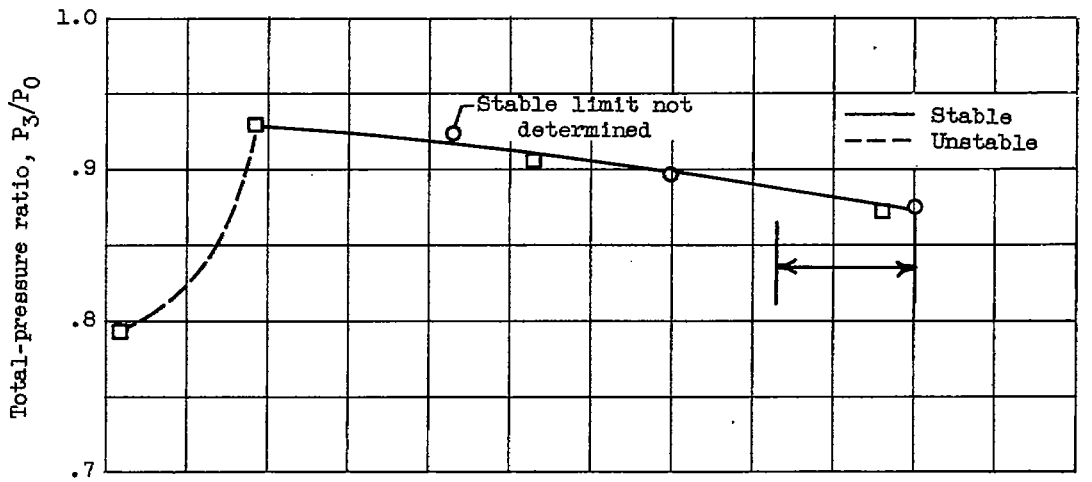

(b) Free-stream Mach number, 1.9.

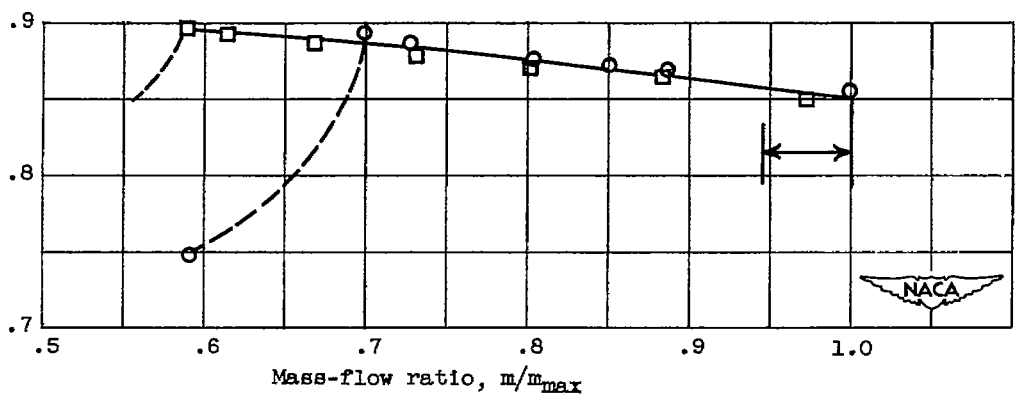

(c) Free-stream Mach number, 2.0.

Figure 3. - Variation of total-pressure recovery with mass-flow ratio; arrows indicate stable range without bleed (reference 1).

[redacted]

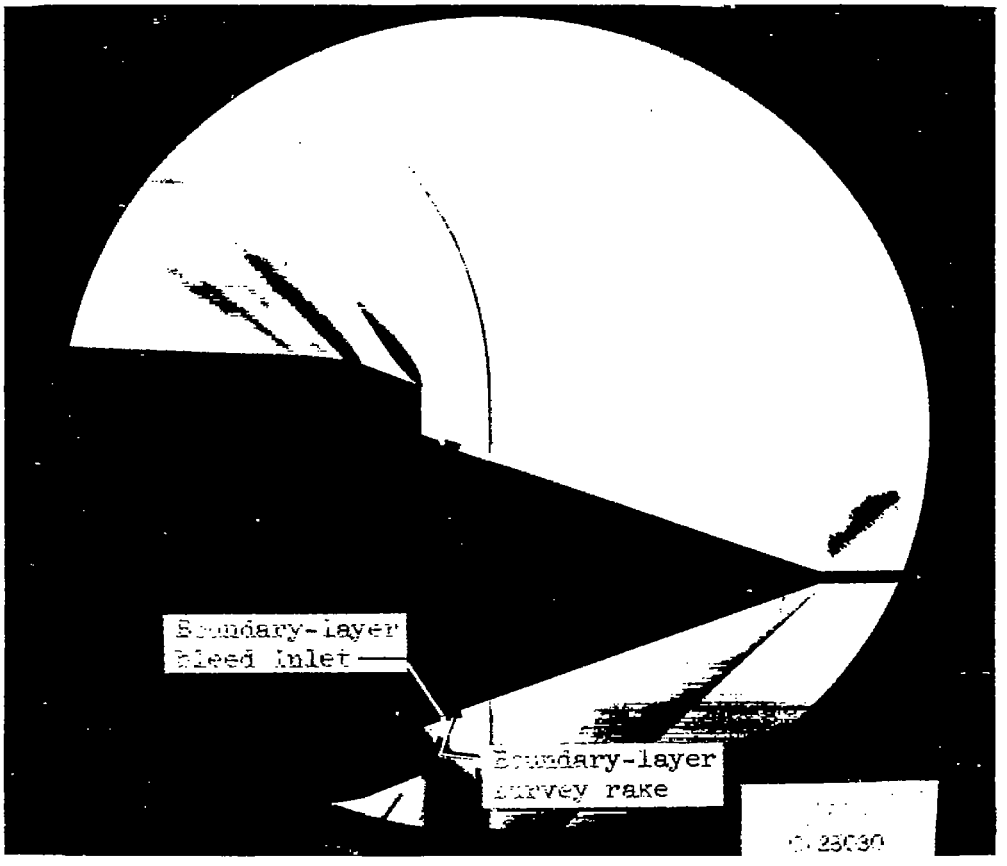

(a) Point A in figure 3; forward lip inlet, $m/m_{max} = 0.677$.

Figure 4. - Schlieren photographs of the inlets for subcritical operation at free-stream Mach number of 1.7.

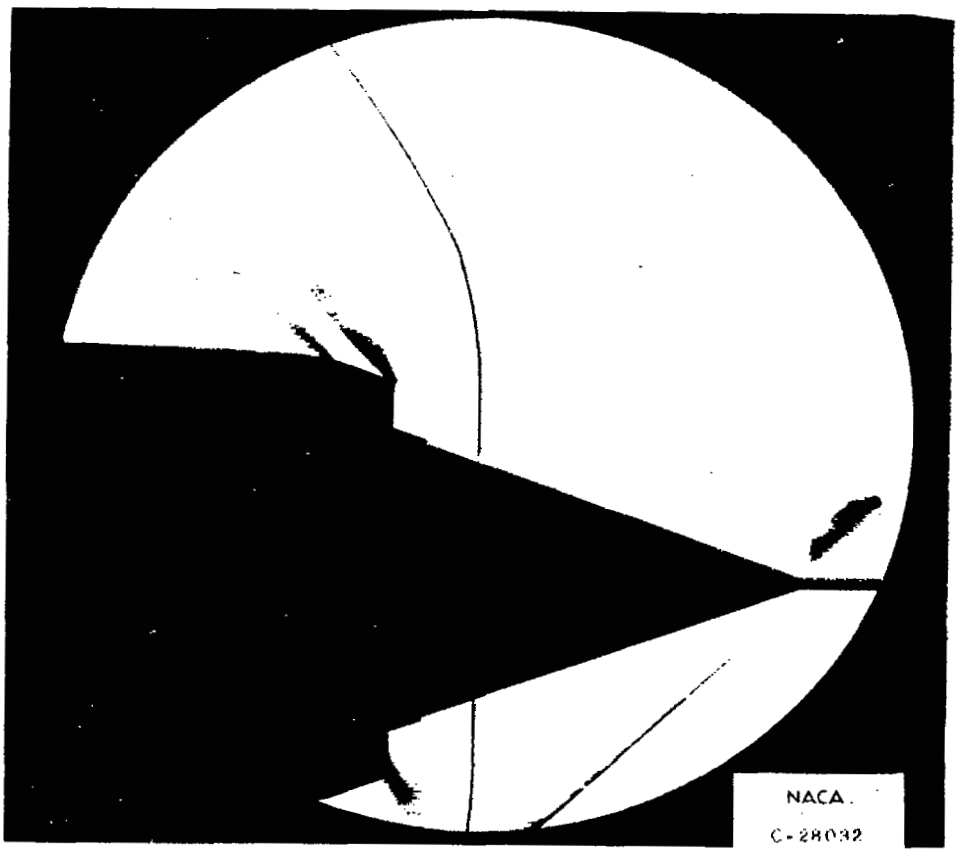

(b) Point B in figure 3; rearward lip inlet, $m/m_{max} = 0.560$.

Figure 4. - Concluded. Schlieren photographs of the inlets for subcritical operation at free-stream Mach number of 1.7.

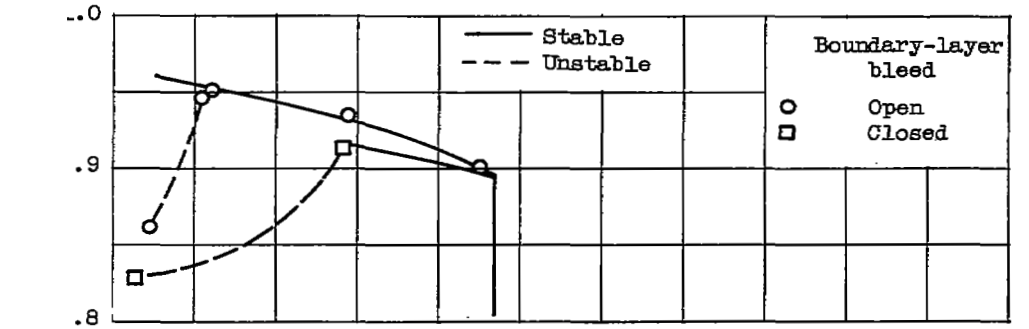

(a) Free-stream Mach number, 1.7.

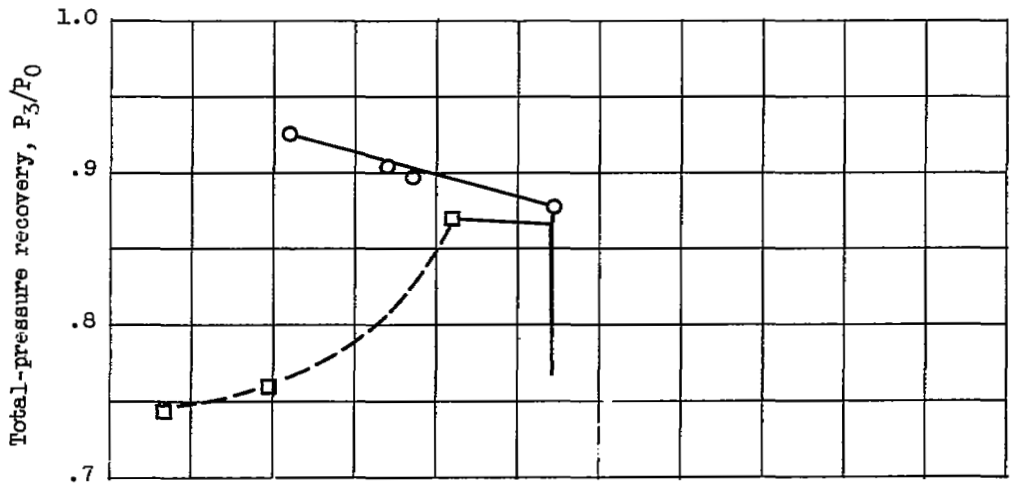

(b) Free-stream Mach number, 1.9.

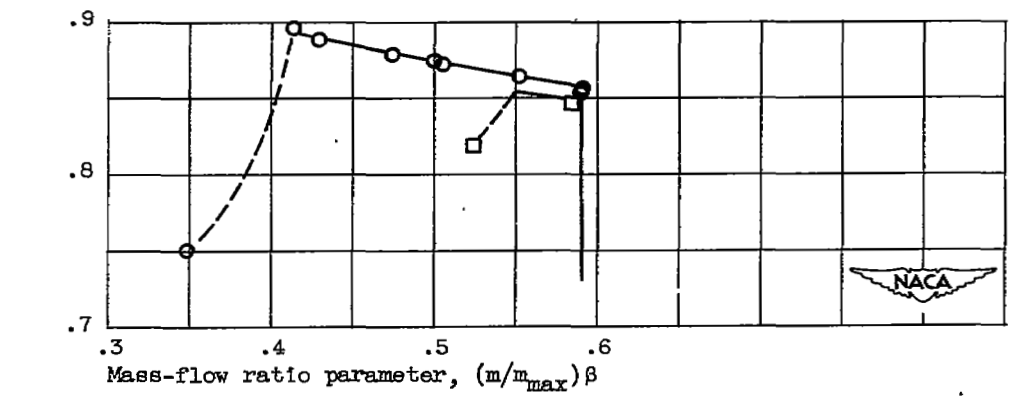

(c) Free-stream Mach number, 2.0.

Figure 5. - Variation of total-pressure recovery with mass-flow ratio parameter for forward lip inlet with boundary-layer bleed opened and closed.

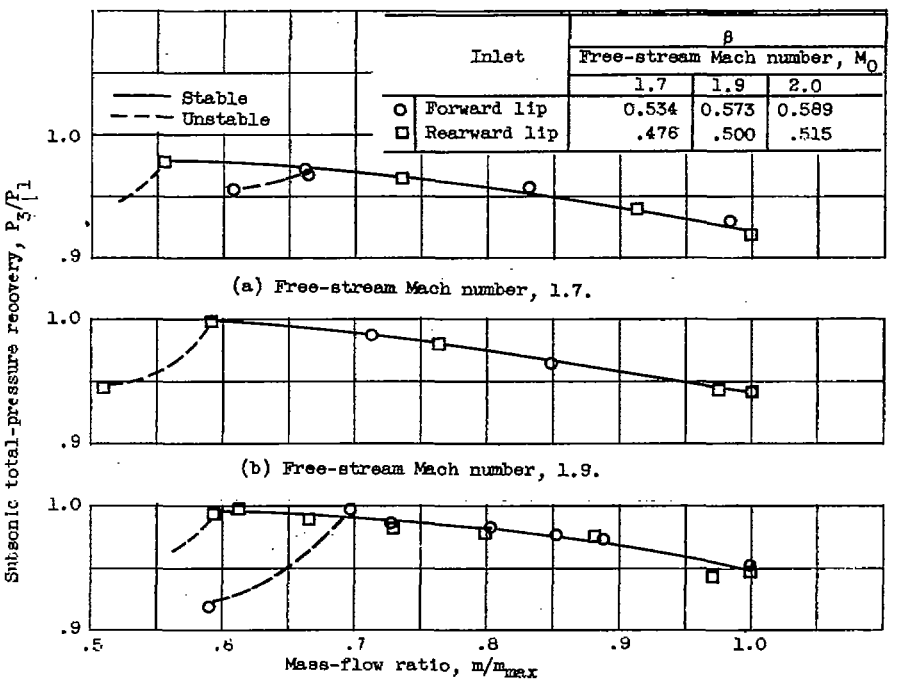

(a) Free-stream Mach number, 1.7.

(b) Free-stream Mach number, 1.9.

(c) Free-stream Mach number, 2.0.

Figure 6. - Variation of total-pressure recovery in subsonic diffuser with mass-flow ratio.

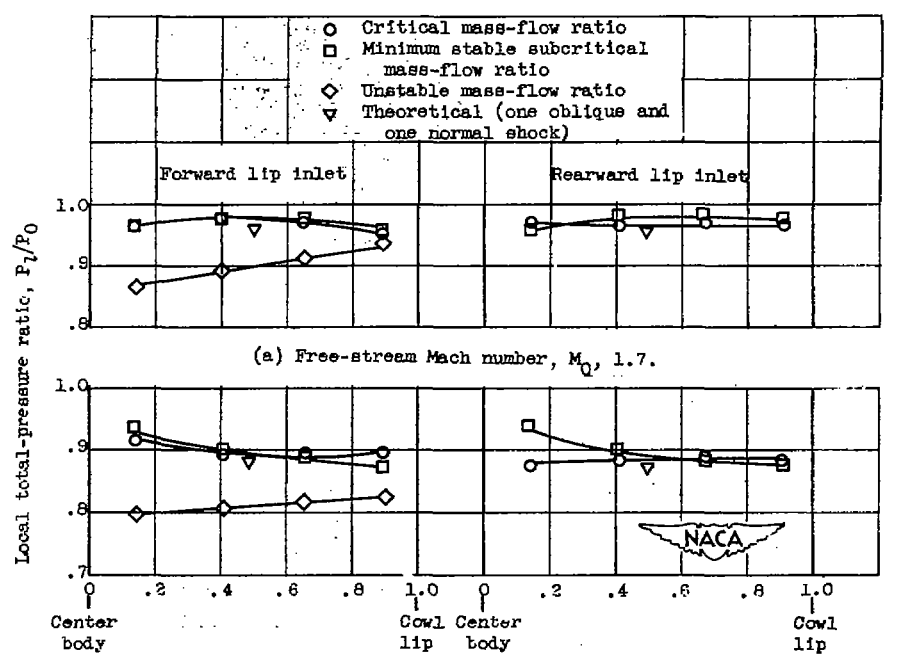

(a) Free-stream Mach number, M_0, 1.7.

(b) Free-stream Mach number, M_0, 2.0.

Figure 7. - Variation of total-pressure profiles across cowl-lip station.

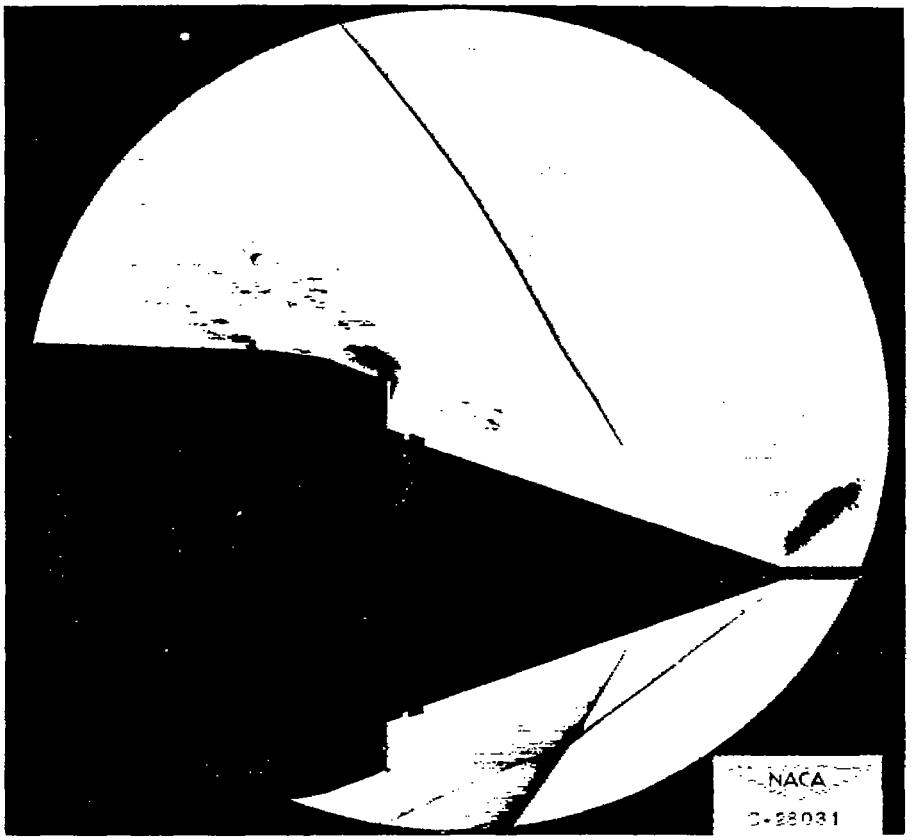

Figure 8. - Schlieren photograph of pulsing condition at free-stream Mach number of 2.0. Exposure, 1 microsecond.

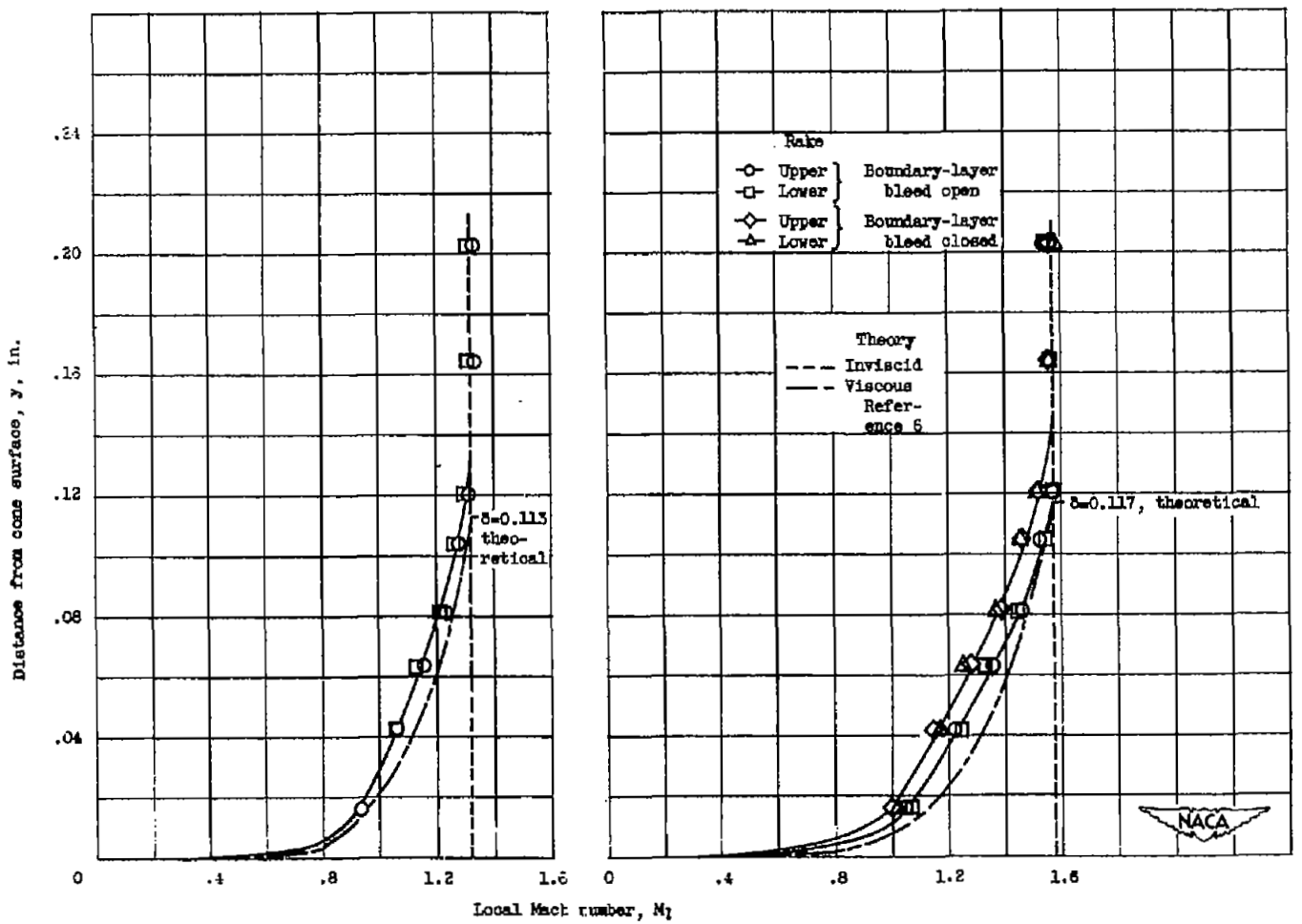

(a) Free-stream Mach number, 1.7.

(b) Free-stream Mach number, 2.0.

Figure 9. - Variation of cone-boundary-layer profiles on forward lip inlet at critical conditions.

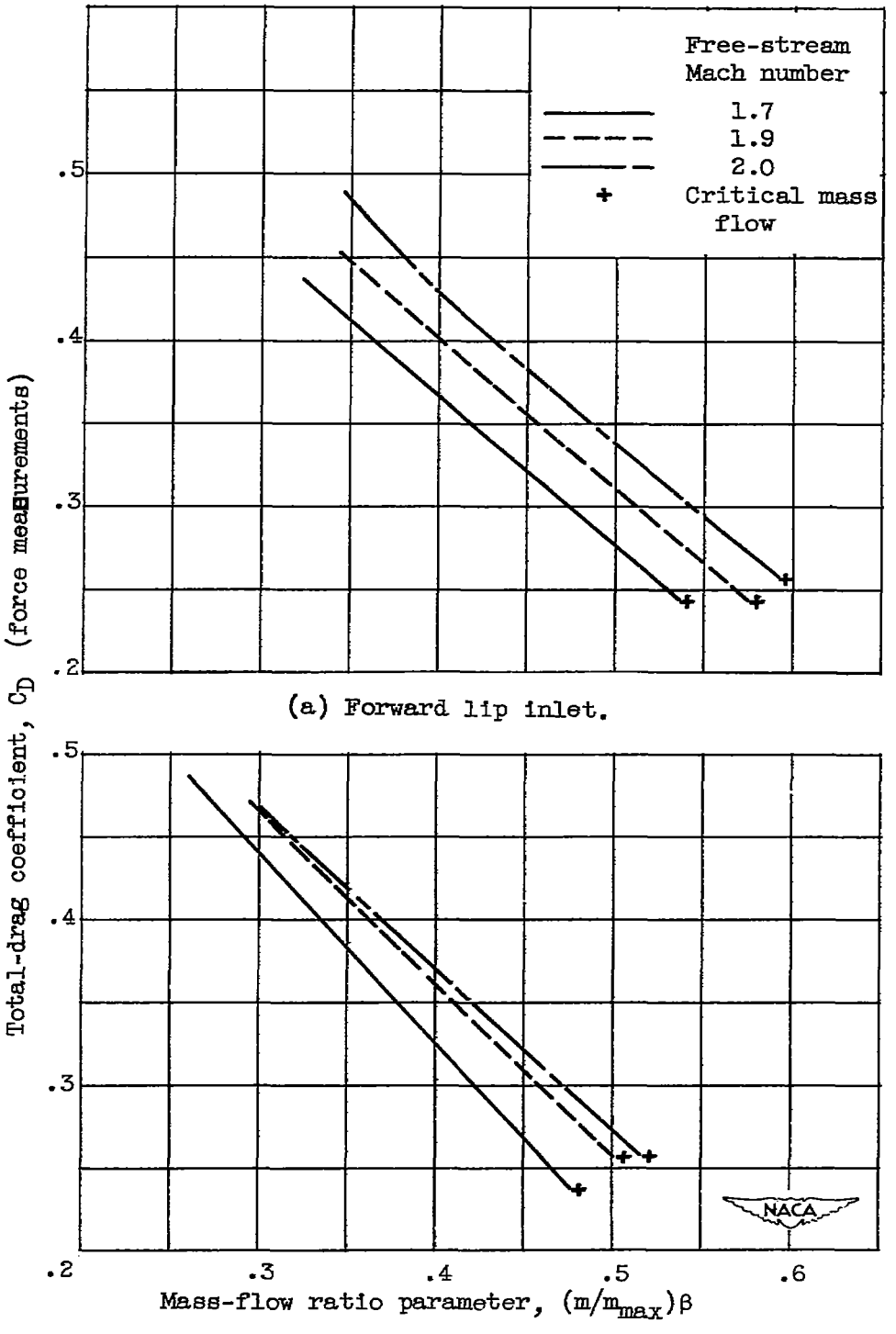

(a) Forward lip inlet.

(b) Rearward lip inlet.

Figure 10. - Variation of drag coefficient with mass-flow ratio parameter.

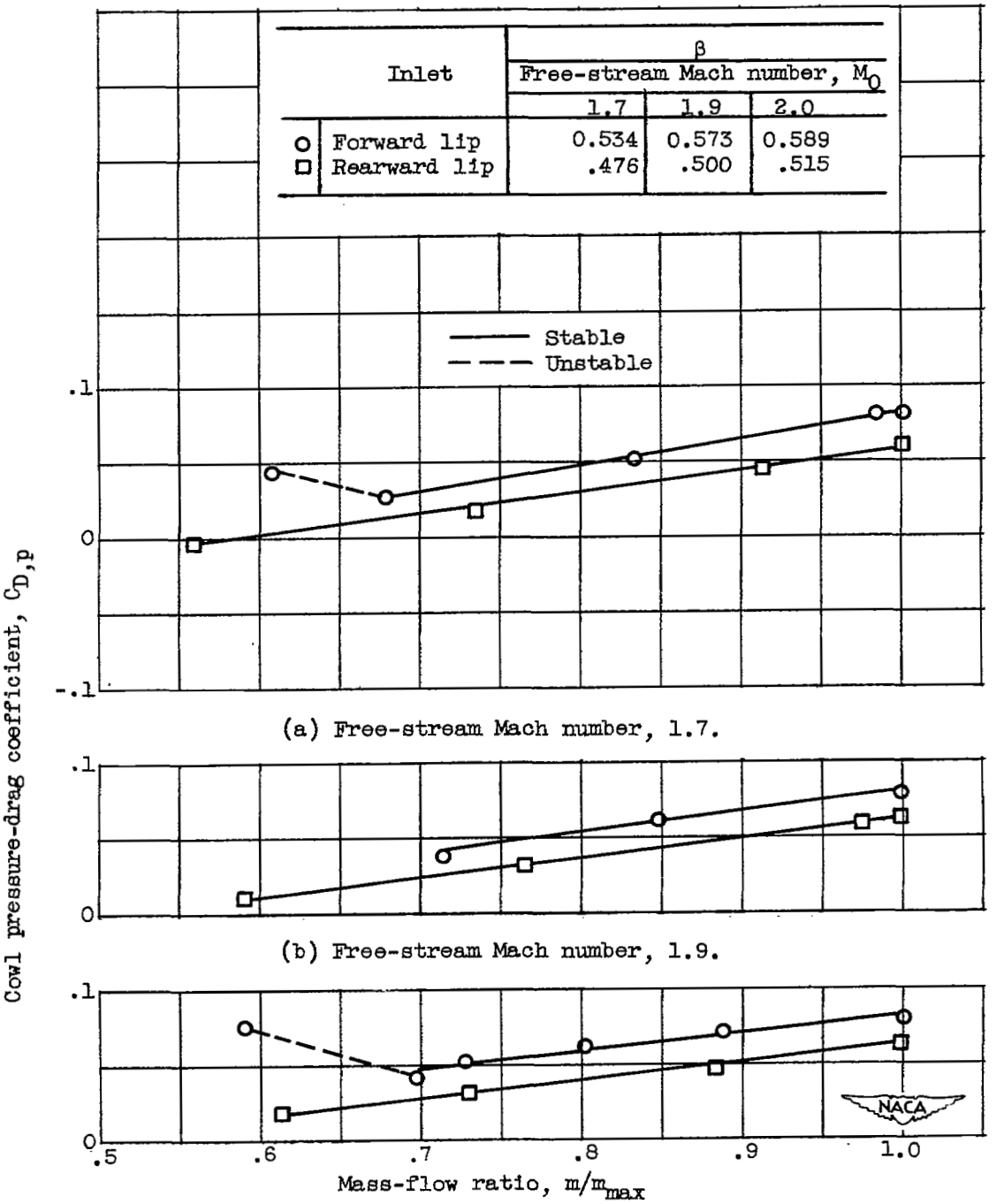

(a) Free-stream Mach number, 1.7.

(b) Free-stream Mach number, 1.9.

(c) Free-stream Mach number, 2.0.

Figure 11. - Variation of cowl pressure-drag coefficient with mass-flow ratio.

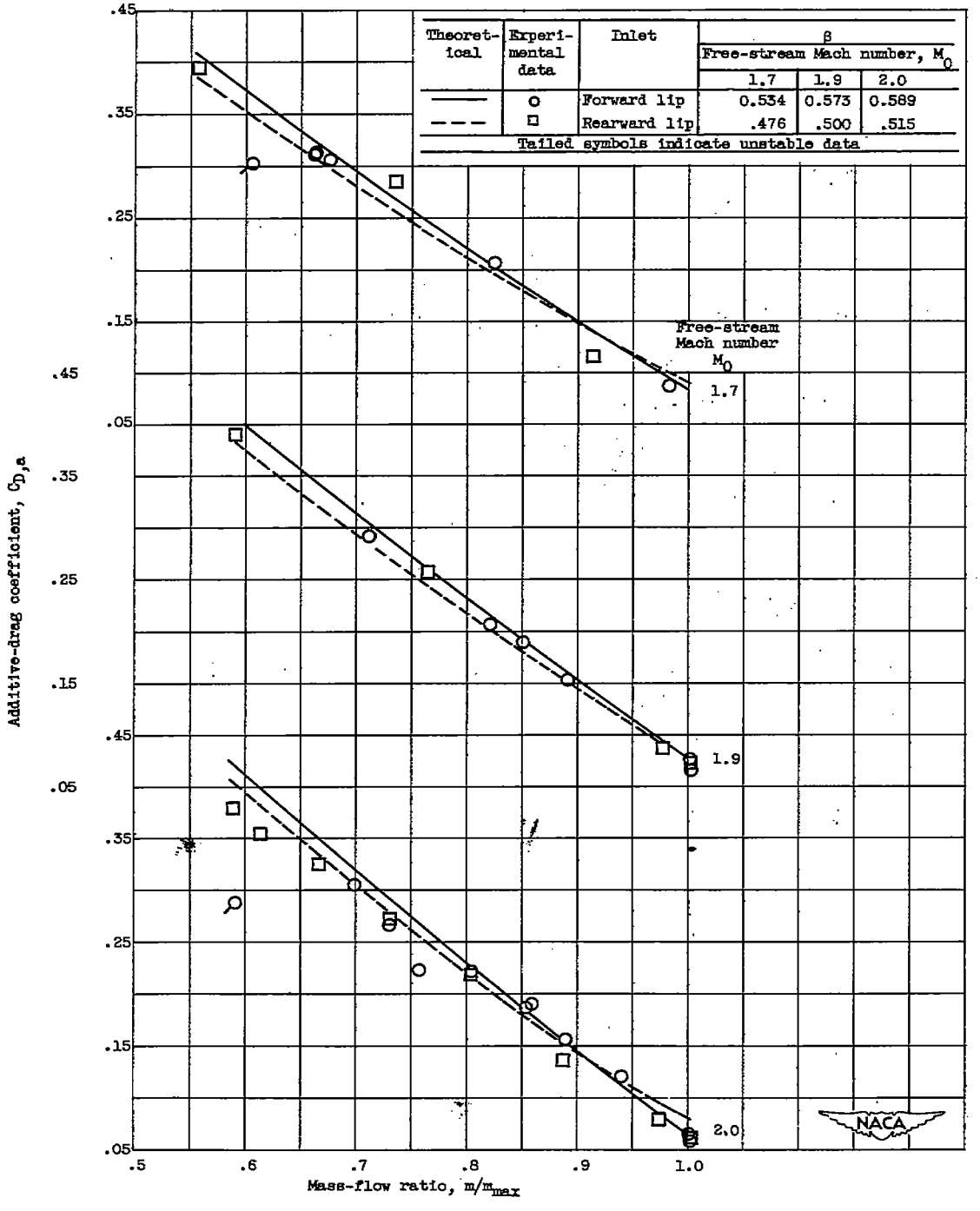

Figure 12. - Theoretical and experimental variation of additive-drag coefficient with mass-flow ratio.

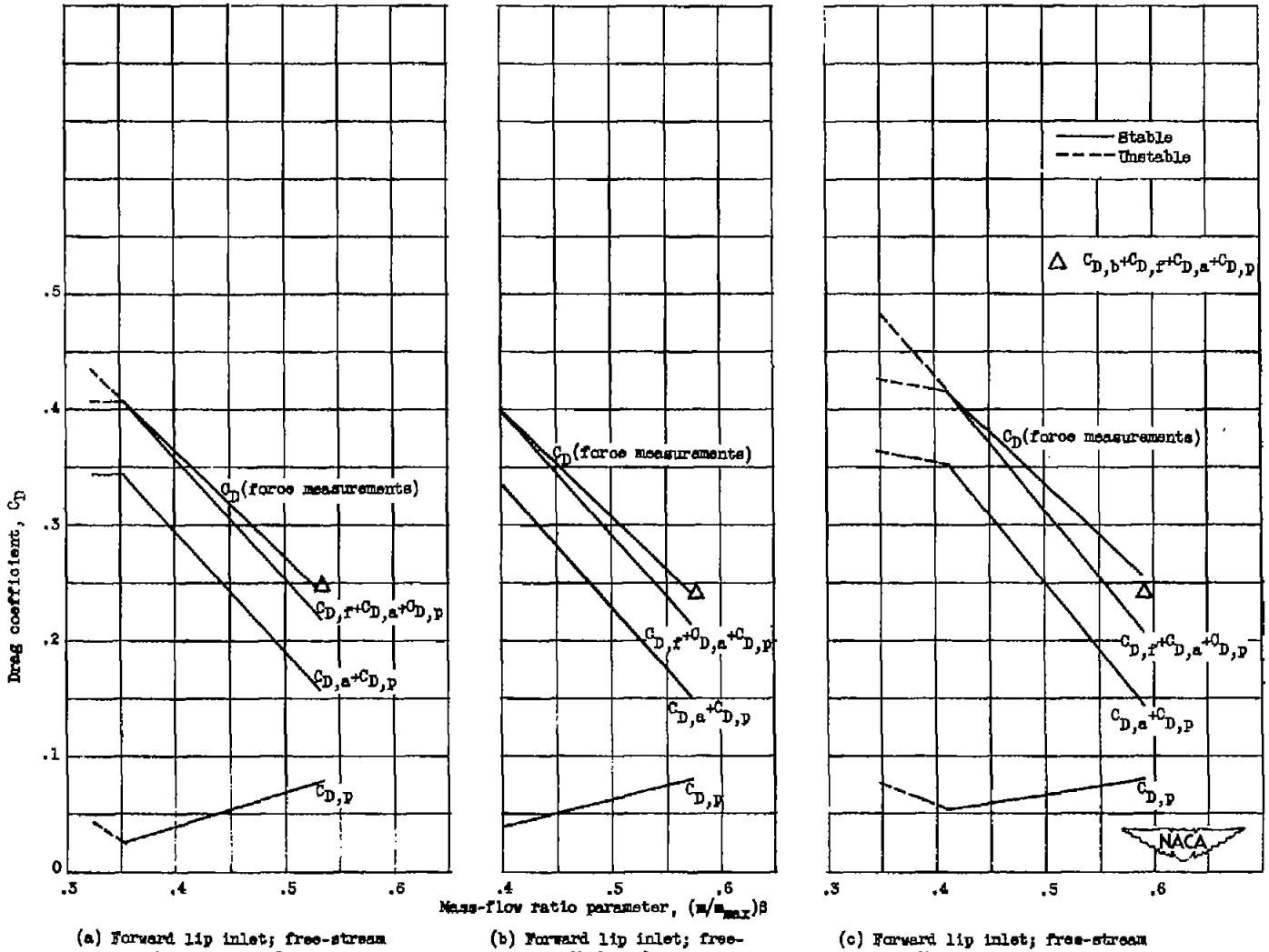

(a) Forward lip inlet; free-stream Mach number, 1.7.

(b) Forward lip inlet; free-stream Mach number, 1.9.

(c) Forward lip inlet; free-stream Mach number, 2.0.

Figure 13. - Variation of components of total drag with mass-flow ratio parameter.

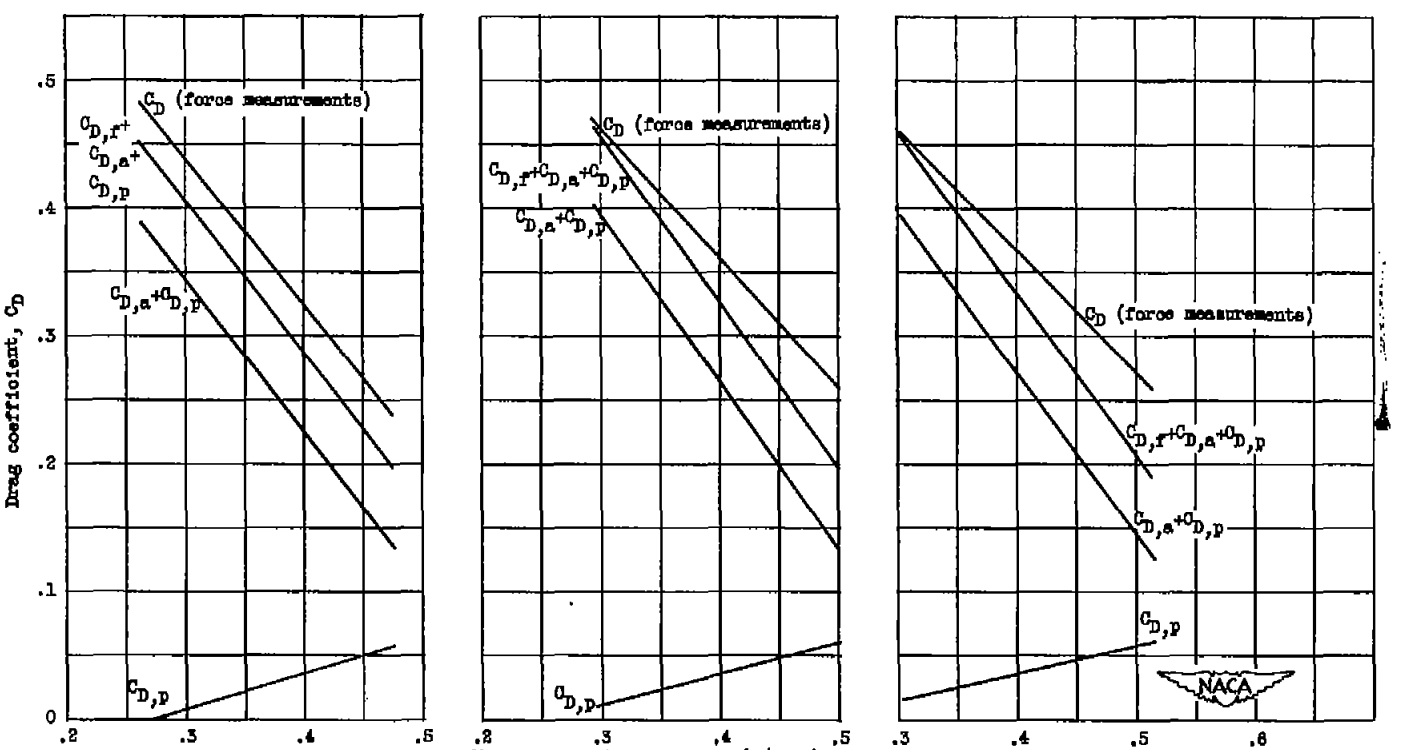

(d) Rearward lip inlet; free-stream Mach number, 1.7.

(e) Rearward lip inlet; free-stream Mach number, 1.9.

(f) Rearward lip inlet; free-stream Mach number, 2.0.

Figure 13. - Concluded. Variation of components of total drag with mass-flow ratio parameter.